CHIN. PHYS. LETT. Vol. 33, No. 1 (2016) 014302

Three-Dimensional Scattering of an Incident Plane Shear Horizontal Guided Wave by a Partly through-Thickness Hole in a Plate *

Wen-Fa Zhu(朱文发)[1,2], Hai-Yan Zhang(张海燕)[1**], Jian Xu(徐建)[1], Xiao-Dong Chai(柴晓冬)[2]

[1]School of Communication and Information Engineering, Shanghai University, Shanghai 200444
[2]School of Urban Railway Transportation, Shanghai University of Engineering Science, Shanghai 201620

(Received 10 September 2015)

We investigate the three-dimensional (3D) scattering problem of an incident plane shear horizontal wave by a partly through-thickness hole in an isotropic plate, in which the Lamb wave modes are also included due to the mode conversions by the scattering obstacle in the 3D problem. An analytical model is presented such that the wave fields are expanded in all of propagating and evanescent SH modes and Lamb modes, and the scattered far-fields of three fundamental guided wave modes are analyzed numerically for different sizes of the holes and frequencies. The numerical results are verified by comparing with those obtained by using the approximate Poisson/Mindlin plate model for small hole radius and low frequency. It is also found that the scattering patterns are different from those of the S0 wave incidence. Our work is useful for quantitative evaluation of the plate-like structure by ultrasonic guided waves.

PACS: 43.20.+g, 43.35.+d DOI: 10.1088/0256-307X/33/1/014302

The potential for exploiting ultrasonic guided waves for the non-destructive testing (NDT) of plate structures has long been recognized and investigated by many researchers.[1–3] The investigation of the wave scattering by defects of various shapes is the top priority of the theory of NDT.[4–7] When guided waves propagate in a plate-like structure with a defect of finite dimensions, the scattering phenomenon occurs. The scattered field describes the effect generated by the presence of the defect on the incident wave field and thus carries all the information related to the defect. The investigation of the scattering problem is of particular interest in the ultrasonic quantitative nondestructive evaluation (QNDE) for detecting and characterizing the location, shape and size of the defect.

Compared with the Lamb waves, shear horizontal (SH) guided waves show more simple dispersion characteristics, which lead to easier signal interpretation and more reliable nondestructive evaluation (NDE). Many analytical and numerical studies on the scattering characteristics of SH guided waves have been reported.[8–12] Early, Wang *et al.*[8] studied the scattering problem of guided SH waves by a partly debonded circular cylinder in a traction-free plate based on the method of expanding the field in a sum of normal wave modes and a series of Chebyshev polynomials. Grahn[9] solved the two-dimensional (2D) scattering problem of an internal crack in a layered anisotropic plate using a Green function approach. Recently, Golub *et al.*[10] have investigated the plane SH-wave propagation in periodically layered elastic composites with a damaged layer. Special focus of the analysis is on the wave reflection and transmissions, band gaps, wave localization and resonance phenomena due to distributed damages. Chen *et al.*[11] have addressed the 2D problem of a time-harmonic plane shear horizontal wave scattered by a finite closed crack in an isotropic material using a spring model. However, all the above-mentioned studies are focused on the 2D scattering problems of SH waves. While 2D investigations can only provide limited insights for the interaction of guided waves with defects, the 3D model is more helpful to fully understand the scattering process.[12]

This Letter is aiming to determining the mode scattering characteristics as the low frequency shear horizontal wave (SH0) mode transmits across a partly through-thickness hole in a plate. In the 3D case, the scattered wave field consists of not only the diffracted SH0 mode, but also contributions of the mode conversion from the S0 and A0 modes. A rigorous 3D model based on Lamb and SH wave equations is used and the validity of the solutions is verified by the approximate Possion/Mindlin plate model.[13] The far-field scattering amplitudes of three fundamental guided wave modes for different hole radii and depths are calculated to show the influence of the defect size upon the scattered wave field. Our work is useful for quantitative evaluation of the plate-like structure by ultrasonic guided waves.

In a cylindrical coordinate system, shear horizontally polarized SH modes can be expressed by using a scalar potential function $\psi(r,\theta)$ and thickness dependent functions $U_n(z)$,[14,15]

$$\begin{aligned} u_r^n &= \frac{1}{l_n} U_n(z) \frac{1}{r} \frac{\partial \psi(r,\theta)}{\partial \theta}, \\ u_\theta^n &= -\frac{1}{l_n} U_n(z) \frac{\partial \psi(r,\theta)}{\partial r}, \\ u_z^n &= 0, \end{aligned} \tag{1}$$

where the scalar potential function $\psi(r,\theta)$ satisfies the Helmholtz equation

$$\frac{\partial^2 \psi}{\partial r^2} + \frac{1}{r}\frac{\partial \psi}{\partial r} + \frac{1}{r^2}\frac{\partial^2 \psi}{\partial \theta^2} + l_n^2 \psi = 0. \tag{2}$$

*Supported by the National Natural Science Foundation of China under Grant Nos 11474195, 11274226, 51478258 and 51405287.
**Corresponding author. Email: hyzh@shu.edu.cn
© 2016 Chinese Physical Society and IOP Publishing Ltd

The wavenumber l_n of the SH mode is given by $l_n^2 = (\frac{\omega}{c_T})^2 - (\frac{n\pi}{2h})^2$, where $n = 0, 2, 4, \ldots$ for symmetric modes and $n = 1, 3, 5, \ldots$ for antisymmetric modes, c_T is the velocity for shear bulk wave, and ω and h are the angular frequency and the half plate thickness, respectively.

An incident guided SH0 wave can be expressed as

$$\psi^{\text{inc}} = e^{il_0^h x_1} = e^{il_0^h r\cos\theta} = \sum_{m=-\infty}^{\infty} i^m J_m(l_0^h r)e^{im\theta}, \quad (3)$$

where the superscript inc stands for the incident wave, l_0^h is the wavenumber of the incident SH0 mode in a plate with thickness $2h$, and $J_m(\cdot)$ are the first kind of Bessel functions. The incident displacement components are obtained via Eqs. (1) and (3), which can be written as

$$\begin{aligned} u_r^{\text{inc}} &= \sum_{m=-\infty}^{\infty} i^{m+1} m U_0^h(z) \frac{J_m(l_0^h r)}{l_0^h r} e^{im\theta}, \\ u_\theta^{\text{inc}} &= \sum_{m=-\infty}^{\infty} -i^m U_0^h(z) J_m(l_0^h r) e^{im\theta}, \\ u_z^{\text{inc}} &= 0. \end{aligned} \quad (4)$$

Employing Hooke's law, the incident stress components for a single SH mode can be written as

$$\begin{aligned} \sigma_{rr}^{\text{inc}} = &\sum_{m=-\infty}^{\infty} i^{m+1} m\mu U_0^h(z) \Big[\frac{2}{r} J'_m(l_0^h r) \\ &- \frac{2}{l_0^h r^2} J_m(l_0^h r)\Big] e^{im\theta}, \end{aligned} \quad (5a)$$

$$\begin{aligned} \sigma_{r\theta}^{\text{inc}} = &\sum_{m=-\infty}^{\infty} i^m \mu U_0^h(z) \Big[\frac{2}{r} J'_m(l_0^h r) \\ &+ \Big(l_0^h - \frac{2m^2}{l_0^h r^2}\Big) J_m(l_0^h r)\Big] e^{im\theta}, \end{aligned} \quad (5b)$$

$$\sigma_{rz}^{\text{inc}} = \sum_{m=-\infty}^{\infty} i^{m+1} m\mu \frac{d}{dz}(U_0^h(z)) \frac{1}{l_0^h r} J_m(l_0^h r) e^{im\theta}. \quad (5c)$$

The expressions of the scattered and transmitted stress and displacement components are the same as those of Ref. [15]. The scattered wave field can be determined by the boundary condition of continuity of displacement and stresses on the surface of the hole, i.e., the sum of the incoming and scattered field equals the transmitted field. The far-field amplitudes are defined as $A_i^\infty(\theta) = |u_i(r,\theta)|\sqrt{r/h}, r \to \infty$, where $u_i(r,\theta)(i = r, \theta, z)$ are the displacement components of S0, SH0 and A0 modes on the surface of the plate, respectively.

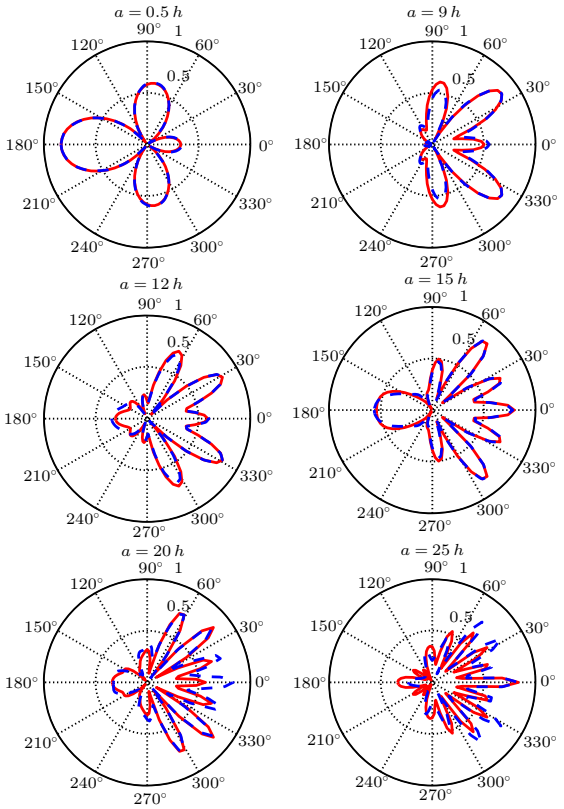

Fig. 1. Far-field scattered amplitudes of the SH0 mode for different hole radii when the SH0 wave is incident on a hole of depth $b/h = 0.5$ at frequency $\Omega = 0.4$: the 3D model (red solid line) and the Poisson/Mindlin model (blue dashed line).

Table 1. Wavenumbers of various modes at the frequency thickness product $fd = 0.4\,\text{MHz·mm}$

Modes	$k_0(l_0)$	$k_1(l_1)$	$k_2(l_2)$	$k_3(l_3)$	$k_4(l_4)$	$k_5(l_5)$	$k_6(l_6)$	$k_7(l_7)$	$k_8(l_8)$	$k_9(l_9)$
S	237	1128 $+2079i$	1152 $+5346i$	1776 $+8530i$	1929 $+11695i$	2047 $+14851i$	2142 $+18002i$	2221 $+21151i$	2290 $+24298i$	2351 $+27444i$
A	730	$543i$	1385 $+3734i$	1676 $+6942i$	1858 $+10114i$	1992 $+13273i$	2097 $+16427i$	2183 $+19577i$	2257 $+22725i$	2322 $+25871i$
SH	400	$1519i$	$3116i$	$4695i$	$6270i$	$7844i$	$9416i$	$10988i$	$12560i$	$14132i$

In the following numerical examples, the steel plate of thickness $d = 2h = 2\,\text{mm}$ with Young's module $E = 210\,\text{GPa}$, Poisson's ratio $\nu = 0.3$ and density $\rho = 8100\,\text{kg/m}^3$ is used. Assume that the blind hole depth $2(h-b)$ is half the plate thickness, i.e., $b = 0.5h$, where $2b$ is the plate thickness below the hole. The incoming field is a plane SH0 wave. Since the wave fields are expressed as superpositions of propagating and evanescent Lamb modes and SH modes in the 3D approach, wavenumbers of these modes can be obtained by the roots of the Rayleigh–Lamb and SH wave equations. Wavenumbers of various modes used in the numerical calculation are listed in Table 1 at the non-dimensional frequency $\Omega = \omega h/c_T = 0.4$, corresponding to the frequency thickness product $fd = 0.4\,\text{MHz·mm}$. In Table 1, the symmetric and asym-

metric Lamb modes are abbreviated to S and A, respectively, and k_n ($n = 0$–9) are the wavenumbers of Lamb modes and l_n ($n = 0$–9) are the wavenumbers of SH modes. The real wavenumbers represent the propagating waves and the complex wavenumber represent the evanescent waves. Notice that there are propagating S0, A0 and SH0 modes at the frequency thickness product $fd = 0.4\,\text{MHz·mm}$.

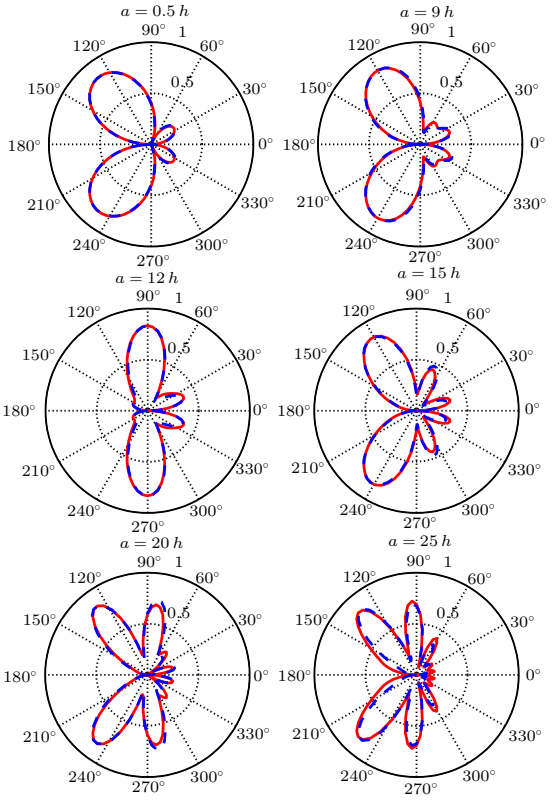

Fig. 2. Far-field scattered amplitudes of the S0 mode for different hole radii when the SH0 wave is incident on a hole of depth $b/h = 0.5$ at frequency $\Omega = 0.4$: the 3D model (red solid line) and the Poisson/Mindlin model (blue dashed line).

For validation of the 3D model, the numerical results based on the appropriate Poisson and Mindlin theories[13] are presented in the following figures. In Figs. 1–6, the far-field scattered amplitudes for the two different models are plotted for different hole radii and frequencies when the SH0 wave is incident on a hole of depth $b/h = 0.5$. It is shown that the agreement between the two models is good for smaller hole radii and at lower frequencies. Evident deviations only occur in the scattering fields for larger hole radii and higher frequencies. The incident SH0 wave can be scattered in 0° and 180° directions, while the converted S0 and A0 waves have almost no components in these directions. These phenomena are different from the case of S0 wave incidence. In Fig. 7, we compare the far-field scattered amplitudes of three modes when the S0 mode is incident on the circular blind hole of radius $a = 12h$ and depth $b/h = 0.3$ at frequency $\Omega = 0.4$. It is shown that S0 and A0 waves are scattered mainly forwards and backwards, while the SH0 wave is scattered mainly in the transverse direction.

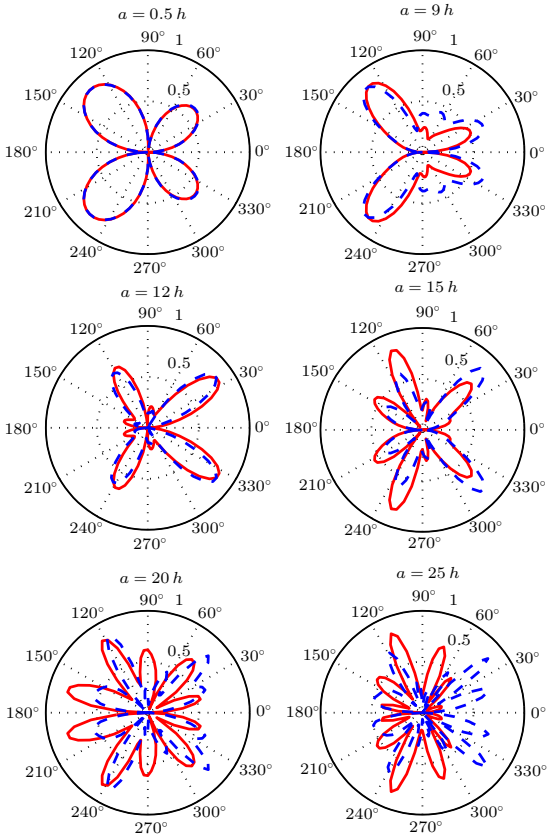

Fig. 3. Far-field scattered amplitudes of the A0 mode for different hole radii when the SH0 wave is incident on a hole of depth $b/h = 0.5$ at frequency $\Omega = 0.4$: the 3D model (red solid line) and the Poisson/Mindlin model (blue dashed line).

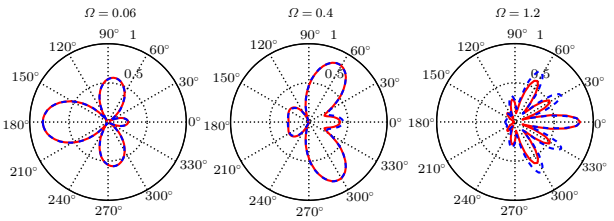

Fig. 4. Far-field scattered amplitudes of the SH0 mode for different frequencies when the SH0 wave is incident on a hole of depth $b/h = 0.5$ and radius $a = 4h$: the 3D model (red solid line) and the Poisson/Mindlin model (blue dashed line).

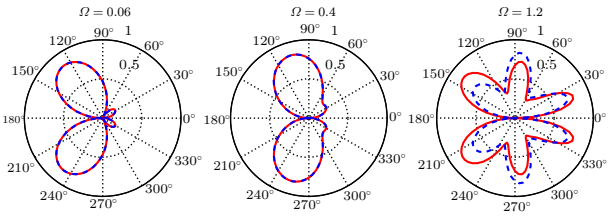

Fig. 5. Far-field scattered amplitudes of the S0 mode for different frequencies when the SH0 wave is incident on a hole of depth $b/h = 0.5$ and radius $a = 4h$: the 3D model (red solid line) and the Poisson/Mindlin model (blue dashed line).

As shown in Figs. 1–6, the scattering profiles of the three modes vary considerably when the hole radius and frequencies are varied. However, the cases for the various hole depth $2(h-b)$ are different. Figures 8–10 show the far-field scattered amplitudes of three funda-

mental modes for different hole depths when the SH0 wave is incident on a hole of radius $a = 4h$ at frequency $\Omega = 0.4$. It is observed that the scattering profiles of the S0 and SH0 waves do not change much except the amplitudes. For the SH0 mode, the wave peaks near the 0° and ±64° scattering angles increase almost linearly with the increase of the hole depth. For the S0 mode, the largest amplitudes near the ±104° scattering angles increase almost linearly with the increase of the hole depth. For the A0 mode, when the hole depth is smaller (corresponding to larger b/h, as $b/h = 0.4$–0.7), similar results with those of S0 and SH0 modes are displayed. When the hole depth is larger, the scattering profiles of A0 mode varies significantly as the hole depth is changed. As shown in Fig. 10, the cases of $b/h = 0.2$ and $b/h = 0.3$ are plotted in red solid and blue dashed lines.

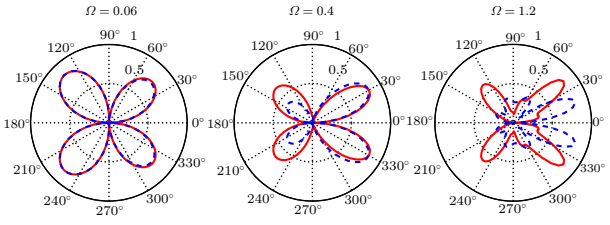

Fig. 6. Far-field scattered amplitudes of the A0 mode for different frequencies when the SH0 wave is incident on a hole of depth $b/h = 0.5$ and radius $a = 4h$: the 3D model (red solid line) and the Poisson/Mindlin model (blue dashed line).

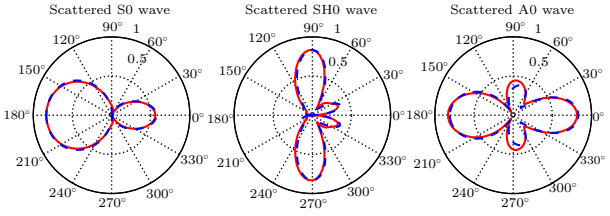

Fig. 7. Far-field scattered amplitudes of three modes when the S0 wave is incident on a hole of radius $a = 12h$ and depth $b/h = 0.5$ at frequency $\Omega = 0.4$: the 3D model (red solid line) and the Poisson/Mindlin model (blue dashed line).

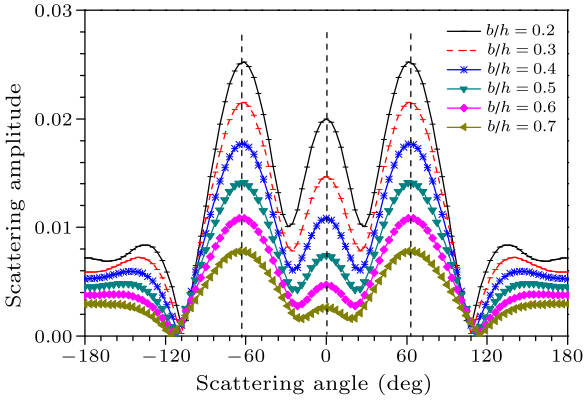

Fig. 8. Far-field scattered amplitudes of the SH0 mode for different hole depths when the SH0 wave is incident on a hole of radius $a = 4h$ at frequency $\Omega = 0.4$.

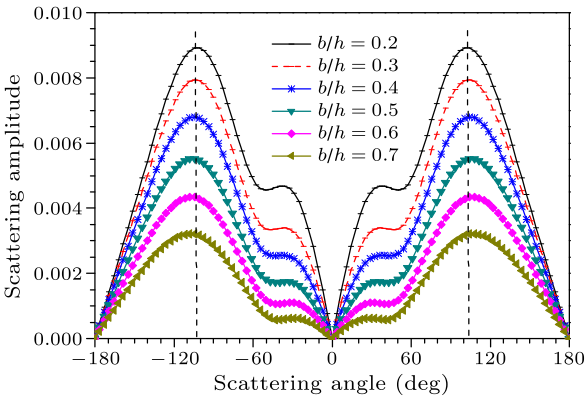

Fig. 9. Far-field scattered amplitudes of the S0 mode for different hole depths when the SH0 wave is incident on a hole of radius $a = 4h$ at frequency $\Omega = 0.4$.

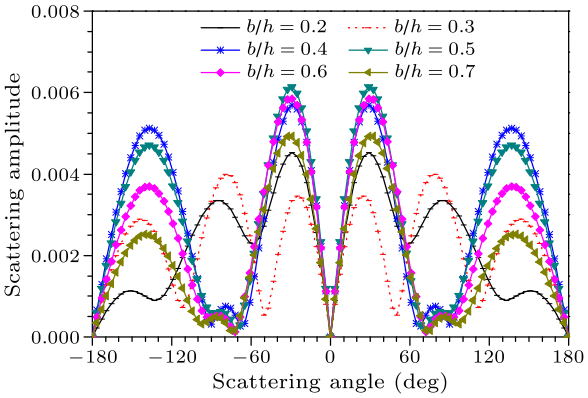

Fig. 10. Far-field scattered amplitudes of the A0 mode for different hole depths when the SH0 wave is incident on a hole of radius $a = 4h$ at frequency $\Omega = 0.4$.

In summary, a rigorous 3D analytical model has been presented for predicting SH0 wave scattering from a partly through-thickness hole in an isotropic plate. The model is verified by comparing with the approximate Poisson/Mindlin model for low frequency and small hole radius. The scattering behaviors of three fundamental guided wave modes for various hole sizes and frequencies are explored, and the results reveal that the far-field scattered patterns of three modes vary considerably when the hole radius and frequency are varied. While the hole depth is varied, the scattering amplitudes of S0 and SH0 modes vary proportionally while the profiles change slightly. For the A0 wave, the profile of the scattering pattern varies significantly for the larger hole depth. In addition, when the incident wave is the SH0 mode, it is observed that the SH0 wave can be scattered almost in all directions, while the converted S0 and A0 waves are scattered mainly in the transverse direction. The phenomena are different from the case of the S0 mode incidence, where the SH0 wave is scattered mainly in the transverse direction and S0 and A0 waves are scattered mainly forwards and backwards. From a practical point of view, these results can provide some guidance for NDE, for example, selecting the appropriate guided mode and measuring direction to achieve maximum sensor response.

References

[1] Chen X, Michaels J E and Michaels T E 2015 *IEEE Trans. Ultrason. Ferro. Freq. Control.* **62** 208
[2] Wang B, Qian Z H and Hirose S 2015 *Shock Vib.* **2015** 1
[3] Zhang H Y, Xu J and Ma S W 2015 *Chin. Phys. Lett.* **32** 084301
[4] Moreau L, Caleap M, Velichko A and Wilcox P D 2012 *Wave Motion* **49** 375
[5] Zhang H Y, Yao J C and Ma S W 2014 *Chin. Phys. Lett.* **31** 034301
[6] Zhang H Y, Yao J C, Wang R and Ma S W 2014 *Chin. Phys. Lett.* **31** 084301
[7] Golato A, Demirli R and Santhanam S 2014 *Wave Motion* **51** 1349
[8] Wang X M and Ying C F 2001 *Sci. Chin.* A **44** 378
[9] Grahn T 2001 *J. Nondestruct. Eval.* **20** 17
[10] Golub M V, Zhang C Z and Wang Y S 2012 *J. Sound Vib.* **331** 1829
[11] Chen B J, Du C L, Zhang J L and Xiao Z M 2013 *Acta Mech.* **224** 2649
[12] Moreau L, Caleap M, Velichko A and Wilcox P D 2011 *Wave Motion* **48** 586
[13] Cegla F B, Rohde A and Veidt M 2008 *Wave Motion* **45** 162
[14] Achenbach J D and Xu Y 1999 *J. Acoust Soc. Am.* **106** 83
[15] Grahn T 2003 *Wave Motion* **37** 63